

Effects of non-linear rheology on the electrospinning process: a model study

Giuseppe Pontrelli^{1a}, Daniele Gentili^a, Ivan Coluzza^a, Dario Pisignano^b, Sauro Succi^a

^a*Istituto per le Applicazioni del Calcolo - CNR, Via dei Taurini 19-00185, Rome, Italy*
tel. +39 0649270927, fax +39 064404306
Email: giuseppe.pontrelli@gmail.com

^b*Dipartimento di Matematica e Fisica "E. De Giorgi", University of Salento & National Nanotechnology Laboratory of Istituto Nanoscienze - CNR, Via Arnesano-73100 Lecce, Italy*

Abstract

We develop an analytical bead-spring model to investigate the role of non-linear rheology on the dynamics of electrified jets in the early stage of the electrospinning process. Qualitative arguments, parameter studies as well as numerical simulations, show that the elongation of the charged jet filament is significantly reduced in the presence of a non-zero yield stress. This may have beneficial implications for the optimal design of future electrospinning experiments.

Keywords: Electrospinning, Herschel-Bulkley, viscoelasticity, stable jet

1. Introduction

The dynamics of charged polymers in external fields is an important problem in non-equilibrium thermodynamics, with many applications in science and engineering [10, 2]. In particular, such dynamics lies at the heart of electrospinning experiments, whereby charged polymer jets are electrospun to produce nanosized fibers; these are used for several applications, as reinforcing elements in composite materials, as building blocks of non-wetting surfaces layers on ordinary textiles, of very thin polymeric separation membranes, and of nanoelectronic and nanophotonic devices [18, 1, 3, 17]. In a typical electrospinning experiment, a charged polymer liquid is ejected at the nozzle and is accelerated by an externally

¹Corresponding author.

applied electrostatic field until it reaches down to a charged plate, where the fibers are finally collected. During the process, two different regimes take place: an initial stable phase, where the steady jet is accelerated by the field in a straight path away from the spinneret (the ejecting apparatus); a second stage, in which an electrostatic-driven bending instability arises before the jet reaches down to a collector (most often a grounded or biased plane), where the fibers are finally deposited. In particular, any small disturbance, either a mechanical vibration at the nozzle or hydrodynamic perturbations within the experimental apparatus, misaligning the jet axis, would lead the jet into a region of chaotic bending instability [21]. The stretching of the electrically driven jet is thus governed by the competition between electrostatics and fluid viscoelastic rheology.

The prime goal of electrospinning experiments is to minimize the radius of the collected fibers. By a simple argument of mass conservation, this is tantamount to maximizing the jet length by the time it reaches the collecting plane. Consequently, the bending instability is a desirable effect, as long it can be kept under control in experiments. By the same argument, it is therefore of interest to minimize the length of the initial stable jet region. Analyzing such stable region is also relevant for an effective comparison with results coming from electrospinning experiments studied in real-time by means of high-speed cameras [6] or X-ray phase-contrast imaging [13].

In the last years, with the upsurge of interest in nanotechnology, electrospinning has made the object of comprehensive studies, from both modelling [7] and experimental viewpoints [23] (for a review see [9]). Two families of models have been developed: the first treats the jet filament as obeying the equations of continuum mechanics [22, 11, 12, 14, 15]. Within the second one, the jet is viewed as a series of discrete elements obeying the equations of Newtonian mechanics [21, 24]. More precisely, the jet is regarded as a series of charged beads, connected by viscoelastic springs. Both approaches above typically assume Newtonian fluids, with a linear strain-stress constitutive relation. On the other hand, in a recent time, the use of viscoelastic fluids has also been investigated in a number of papers, both theoretical and experimental, for the case of power-law [11, 22] and other viscoelastic fluids [7, 8], with special attention to the instability region.

In this paper, we investigate the effects of Herschel-Bulkley non-Newtonian rheology on the early stage of the jet dynamics. The main finding is that the jet elongation during such initial stable phase can be considerably slowed down for the case of yield-stress fluids. As a result, the use of yield-stress fluids might prove beneficial for the design of future electrospinning experiments.

2. The model problem

Let us consider the electrical driven liquid jet in the electrospinning experiment. We confine our attention to the initial rectilinear stable jet region and, for simplicity, all variables are assumed to be uniform across the radial section of the jet, and vary along z only, thus configuring a one-dimensional model. The filament is modelled by two charged beads (*dimer*) of mass m and charge e , separated by a distance l , and subjected to the external electrical field V_0/h , h being the distance of the collector plate from the injection point (Fig. 1) and V_0 the applied voltage.

The deformation of the fluid filament is governed by the combined action of electrostatic and viscoelastic forces (gravity and surface tension are neglected), so that the momentum equation reads [21]:

$$m \frac{dv}{dt} = -\frac{e^2}{l^2} + \frac{eV_0}{h} + \pi a^2 \sigma, \quad (2.1)$$

where a is the cross-section radius of the bead and v the velocity defined as:

$$\frac{dl}{dt} = -v \quad (2.2)$$

For a viscoelastic fluid, the stress σ is governed by the following equation:

$$\frac{d\sigma}{dt} = -\frac{1}{\tau} (\sigma - \sigma_{HB}), \quad (2.3)$$

where τ is the time relaxation constant and σ_{HB} is the Herschel-Bulkley stress [16, 5] that reads

$$\sigma_{HB} = \sigma_Y + K \left(\frac{dl}{l dt} \right)^n \quad (2.4)$$

In the previous expression, σ_Y is the yield stress, n is the power-law index and $\mu_0 = K \left| \frac{1}{l} \frac{dl}{dt} \right|^{n-1}$ is the effective viscosity with K a prefactor having dimensions $gs^{n-2}cm^{-1}$; the case $n = 1$ and $\sigma_Y = 0$ recovers the Maxwell fluid model, with $\mu_0 \equiv const.$ In the stress eqns. (2.3)–(2.4), the Maxwell, the power-law and the Herschel-Bulkley models are combined. A large class of polymeric and industrial fluids are described by $\sigma_Y > 0$ (Bingham fluid) and $n < 1$ (shear-thinning fluid), $n > 1$ (shear-thickening fluid) [4, 19, 20].

It is expedient to recast the above eqns. in a nondimensional form by defining a length scale and a reference stress as in [21]:

$$L = \left(\frac{e^2}{\pi a_0^2 G} \right)^{\frac{1}{2}} \quad G = \frac{\mu_0}{\tau} \quad (2.5)$$

with a_0 the initial radius. With no loss of generality, we assume the initial length of the dimer to be L . Space is scaled in units of the equilibrium length L at which Coulomb repulsion matches the reference viscoelastic stress G , while time is scaled with the relaxation time τ . The following nondimensional groups:

$$Q = \frac{e^2 \mu_0^2}{L^3 m G^2} \quad V = \frac{e V_0 \mu_0^2}{h L m G^2} \quad F = \frac{\pi a_0^2 \mu_0^2}{L m G} \quad (2.6)$$

measure the relative strength of Coulomb, electrical, and viscoelastic forces respectively [21]. Note that the above scaling implies $F = Q$. By setting $W = -v$ and applying mass conservation:

$$\pi a^2 l = \pi a_0^2 L$$

the above equations (2.1)–(2.4) take the following nondimensional form:

$$\begin{aligned} \frac{dl}{dt} &= W \\ \frac{dW}{dt} &= V + Q/l^2 - F\sigma/l \\ \frac{d\sigma}{dt} &= \sigma_Y + (W/l)^n - \sigma \end{aligned} \quad (2.7)$$

with initial conditions: $l(0) = 1, W(0) = 0, \sigma(0) = 0$. Eqs. (2.7) describe a dynamical system with non-linear dissipation for $n \neq 1$. It can conveniently be pictured as a particle rolling down the potential energy landscape $E(l) = Q/l - Vl$. Since the conservative potential is purely repulsive, the time-asymptotic state of the system is escape to infinity, i.e. $l \rightarrow \infty$ as $t \rightarrow \infty$. However, because the system also experiences a non-linear dissipation, its transient dynamics is non-trivial. This may become relevant to electrospinning experiments, as they take place in set-up about and below 1 meter size, so that transient effects dominate the scene.

Before discussing numerical results, we firstly present a qualitative analysis of the problem.

3. Qualitative analysis

In the following we discuss some metastable and asymptotic regimes associated with the set of eqs. (2.7) for $\sigma_Y = 0$ and $n = 1$ for simplicity, even though the qualitative conclusions apply to the general case as well (sect. 4).

Accelerated expansion: free-fall

In the absence of any Coulomb interaction and viscous drag ($Q = F = 0$), the particle would experience a free-fall regime

$$l(t) = l_0 + W_0 t + V t^2 / 2 = l_0 + V t^2 / 2 \propto t^2 \quad (3.1)$$

for $t \gg 1$. The same regime would be attained whenever Coulomb repulsion comes in exact balance with stress pullback, i.e.,

$$\sigma = \frac{Q}{Fl} = \frac{1}{l} \quad (3.2)$$

Since $\frac{d^2 l}{dt^2} = V$, one has $\sigma \rightarrow 1/t^2$ as $l \rightarrow \infty$, configuring again accelerated free-fall as the time-asymptotic regime of the system.

Linear expansion

Another possible scenario is the linear escape, i.e. $\frac{dW}{dt} = 0$, yielding:

$$l(t) \propto t \quad (3.3)$$

This is obtained whenever the viscous drag exceeds over the Coulomb repulsion by just the amount supplied by the external field V , namely:

$$\sigma = \frac{Q/l + Vl}{F} = \frac{1}{l} + \frac{V}{Q} l \quad (3.4)$$

leaving $\frac{d^2 l}{dt^2} = 0$. This shows that, in order to sustain a linear growth, the stress should diverge linearly with the dimer elongation. Again, this is incompatible

with any asymptotic state of the stress evolution. However, if V is sufficiently small, namely:

$$l < l_Q = (Q/V)^{1/2} \quad (3.5)$$

such regime may be realized on a transient basis. Note that l_Q designates the length below which Coulomb repulsion prevails over the external field.

As we shall show, the solution $l \sim t$, $\sigma \sim 1/l \sim 1/t$ can indeed be attained as a transient quasi-steady state regime. Typical experimental values are $Q/V \sim 10$, so that $l_Q \sim 3 - 10$ indicating that such regime could indeed be attained in experiments with elongations $l < 1 - 3$ cm (see section 4). Note that the value of l_Q is independent of the rheological model, this latter affecting however the time it takes to reach the condition $l = l_Q$. To analyze this issue, let us consider the steady-state limit of the stress equation for a generic value of the exponent n , i.e.

$$\sigma = \left(\frac{1}{l} \frac{dl}{dt} \right)^n \quad (3.6)$$

The solution $l(t) \sim t$ delivers $\sigma \sim t^{-n} \sim l^{-n}$, which is indeed compatible with the condition (3.4) for the case $n = 1$. Of course this is not an exact solution, since $\frac{d\sigma}{dt} = 0$ implies $\sigma = \text{const}$ in time. However, it can be realized as a quasi-solution, in the sense that $\frac{1}{\sigma} \frac{d\sigma}{dt} \ll 1$.

The above analysis is relevant because electrospinning experiments take place under finite-size and finite-time non-equilibrium conditions, and it is therefore of great interest to understand the transition time between the two regimes. In particular, the bending instability leading to three-dimensional helicoidal structures sets in after an initial stage in which the polymer jet falls down in a linear configuration. Since the goal of the experiment is to maximize the length l of the polymer fiber by the time it reaches the collector plate, it appears instrumental to trigger the bending instability as soon as possible, so as minimize the elongation of the initial stable jet. The present study is essentially a parametric analysis of this initial stage.

4. Numerical results

We have integrated the system of eqs (2.7) with a velocity-Verlet like time marching scheme:

$$\begin{aligned}
\hat{l} &= l + W\Delta t + a\frac{\Delta t^2}{2} \\
\sigma_{HB} &= \left(\frac{2W}{\hat{l} + l}\right)^n + \sigma_Y \\
\hat{\sigma} &= e^{-\Delta t} \sigma + (1 - e^{-\Delta t})\sigma_{HB}; \\
\hat{a} &= V - F\frac{\hat{\sigma}}{\hat{l}} + \frac{Q}{\hat{l}^2} \\
\hat{W} &= W + \left(\frac{\hat{a} + a}{2}\right)\Delta t
\end{aligned}$$

with Δt the time step and boundary conditions $l(0) = 1$, $W(0) = \sigma(0) = 0$. Energy conservation has been checked and found to hold up to the sixth digit for simulations lasting up to 10^6 time steps.

Reference results in Maxwell fluid

As a reference case, we first consider the Maxwellian case $n = 1$, $\sigma_Y = 0$ and the typical values of experimental relevance are $L \sim 0.3$ cm, $\tau = 10^{-2}$ s, yielding $Q = F = 12$, $V = 2$. In fig. 2 we report the time evolution of the elongation $l(t)$ and the velocity $W(t)$ (left), along with the stress $\sigma(t)$ and the strain rate W/l (right). Three dynamic regimes are apparent. First, an early transient, characterized by the build-up of velocity under the Coulomb drive and, to a much lesser extent, the external field as well. As a result, the strain rate W/l begins to grow, thus promoting a build-up of the stress, which peaks at about $t = 1.5$. Subsequently, the stress starts to decay due to viscoelastic relaxation. During the burst of the stress, lasting about up to $t = 2$, the velocity comes to nearly constant value, realizing the linear regime discussed in the previous section. However, such regime cannot last long because the stress falls down very rapidly in time and is no longer able of sustain the expanding "pressure" of the electrostatic interactions. As clearly visible in figure 3, the Coulomb repulsion falls down faster than the viscoelastic drag, and consequently the subsequent dynamics is dominated by the external field, which promotes the quadratic scaling $l \sim t^2$, clearly observed in Fig. 2 at $t \gg 2$. When both Coulomb repulsion and viscoelastic drag fall down to negligible values, which is seen to occur at about $t = 5$ (50 ms in physical time), the free-fall regime sets in. At this time, the elongation has reached about $l = 30$, corresponding to approximately 10 cm in physical units. Taking $h = 20$ cm as a reference value for the typical size of the experiment, it is observed that the con-

dition $l = h$ would be reached roughly at $t = 8$, namely 0.1 s, corresponding to a mean velocity of about 2 m/s, fairly comparable with the experimental values.

It is now of interest to explore to what extent such a picture is affected by the fluid material properties. In particular, we wish to investigate whether a non-Newtonian rheology is able to slow down the elongation dynamics, thereby reducing the stable jet length.

Effect of the shear-thinning and shear-thickening

To this purpose, the above simulations have been repeated for different values of $0.2 < n < 1.8$, still keeping $\sigma_Y = 0$. In Fig. 4, we report l, W, σ and the total force F_{tot} as a function of time, for $n = 0.2, 1, 1.8$. As one can see, the former case delivers the fastest growth. This can be understood by noting that in the early stage of the evolution $W/l > 1$ (see Fig. 4), hence $n < 1$ lowers (resp. $n > 1$ raises) the stress contribution as compared to the Maxwellian case, $n = 1$. To be noted that in the transient $1 < t < 2$, at $n = 1.8$, the viscoelastic drag is able to produce a mildly decreasing velocity $W(t)$. However, such mild decrease is very ephemeral, and is quickly replaced by a linear growth like for the other values of n . It is worth to note that for the case $n = 0.2$, the stress remains substantial even at large times, which is reasonable because at $t \gg 1$ s $W/l \ll 1$. However, the impact on the dimer elongation, l , is very mild, because the factor $1/l$ makes the stress fairly negligible as compared to the external field. The final result is that the overall effect of n on the dimer elongation is very mild, of the order of ten percent at most. Hence the power-law model at zero yield-stress has a negligible effect on the jet length.

Influence of the yield stress

In the following, we investigate the effect of a non-zero yield stress, with fixed $n = 1.8$ for convenience. The condition $\sigma_Y > 0$ is expected to slow down the growth of $l(t)$, because the stress decays to a non-zero value even in the infinite time limit.

Fig. 5 shows the time evolution of l, W, σ and F_{tot} , for $\sigma_Y = 0.2, 0.5, 0.8$. From this figure, it is readily appreciated that, at variance with the previous case, increasing values of σ_Y turn out to produce a significant slow down of the fluid elongation. In all case, the velocity $W(t)$ shows a decreasing trend in the transient $1 < t < 2$, coming very close to zero at $t \sim 2.5$ for the case $\sigma_Y = 0.8$. The onset of the free-fall regime is significantly delayed, and consequently, so is the evolution of the dimer elongation, which at $t = 10$ reaches the values $l = 80, 60, 30$ for $\sigma_Y = 0.2, 0.5, 0.8$, respectively. The latter case corresponds to a physical length

of about 10cm , about three times shorter than in the Maxwell case, corresponding to about $l = 90$ at $t = 10$. Hence, we conclude that yield stress fluids may experience a noticeable reduction of the stable jet length in actual electrospinning experiments.

Effective Forces

Finally, it is of interest to inspect the effective force exerted upon the dimer as a function of its elongation. By effective force, we imply the sum of Coulomb repulsion and viscoelastic drag, namely

$$F_{eff}(l) = Q \left(\frac{1}{l^2} - \frac{\sigma(l)}{l} \right) \quad (4.1)$$

This expression may indeed provide useful input to coarse-grained models for three-dimensional simulations of the jet dynamics. The effective force for different values of the exponent n and yield-stress values σ_Y is shown in Fig. 6, left and right panels. From these figures, it is appreciated that the behavior of F_{eff} as a function of the elongation l is similar to its dependence on time, although more peaked around the minimum. Such a minimum occurs slight above the crossover length, l_X at which Coulomb repulsion and viscoelastic drag come to an exact balance, i.e

$$l_X \sigma(l_X) = 1 \quad (4.2)$$

For $l < l_X$ Coulomb repulsion is dominant, thus driving the stretching of the jet. Subsequently, at $l > l_X$ the attractive component (drag) takes over, so that $F_{eff}(l) < 0$, until a minimum is reached, $F_{min} \equiv F(l_{min}) < 0$. Finally, for $l > l_{min}$, the force starts growing again to attain its asymptotic zero value at $l \rightarrow \infty$. For the present choice of parameters, the minimum length l_{min} is not far from the characteristic length $l_Q = \left(\frac{Q}{V} \right)^{1/2}$ (see eqn. (3.5)). With the numerical values in point, $Q = 12$ and $V = 2$, we compute $l_Q \sim 2.44$. Furthermore, such minimum length l_{min} appears to be a decreasing function of n at a given σ_Y and independent of σ_Y at a given n .

It is interesting to note that, upon rescaling the elongation with the computed values $l_{min}(n)$, the three curves with $n = 0.2, 1.0, 1.8$ collapse to a universal function $F_{eff}(l) = A_n f(l/l_{min}(n))$, where A_n is a scaling amplitude which depends on the exponent n . Such universal function might prove useful in the parametrization of three-dimensional interactions.

5. Conclusions

Summarizing, we have developed a model for the flow of electrically charged viscoelastic fluids, with the main aim of investigating the role of non-Newtonian rheology on the stretching properties of electrically charged jets. The simulations show good agreement with the theoretical analysis and provide a qualitative understanding of the role of viscoelasticity in the early stage of the electrospinning experiment. The main finding is that yield-fluids may lead to a significantly reduction of the linear extension of the jet in the initial stage of the electrospinning process. The present findings may also prove useful to set up the model parameters that control the efficiency of the process and the quality of the spun fibers.

Acknowledgments

The research leading to these results has received funding from the European Research Council under the European Unions Seventh Framework Programme (FP/2007-2013)/ERC Grant Agreement n. 306357 (ERC Starting Grant NANO-JETS). One of the authors (S.S.) wishes to thank the Erwin Schroedinger Institute in Vienna, where this work was initiated, for kind hospitality and financial support through the ESI Senior Fellow program.

References

- [1] Agarwal, S., Greiner, A., Wendorff, J., 2013. Functional materials by electrospinning of polymers. *Prog. Polym. Sci.* 38, 963–991.
- [2] Andrady, A., 2008. *Science and technology of polymer nanofibers*. Wiley & Sons.
- [3] Arinstein, A., Burman, M., Gendelman, O., Zussman, E., 2007. Effect of supramolecular structure on polymer nanobre elasticity. *Nat. Nanotechnol.* 2, 59–62.
- [4] Bird, R., Armstrong, R., Hassager, O., 1987. *Dynamics of polymeric liquids*. vol. 1: Fluid mechanics.
- [5] Burgos, G., Alexandrou, A., Entov, V., 1999. On the determination of yield surfaces in Herschel–Bulkley fluids. *Journal of Rheology* 43 (3), 463–483.

- [6] Camposeo, A., Greenfeld, I., Tantussi, F., Pagliara, S., Moffa, M., Fuso, F., Allegrini, M., Zussman, E., Pisignano, D., 2013. Local mechanical properties of electrospun fibers correlate to their internal nanostructure. *Nano Lett.* 13, 5056–5062.
- [7] Carroll, C., Joo, Y., 2006. Electrospinning of viscoelastic Boger fluids: Modeling and experiments. *Physics of Fluids* 18 (5), 053102.
- [8] Carroll, C., Joo, Y., 2011. Discretized modeling of electrically driven viscoelastic jets in the initial stage of electrospinning. *Journal of Applied Physics* 109 (9), 094315.
- [9] Carroll, C., Zhmayev, Eand Kalra, V., Joo, Y., 2008. Nanofibers from electrically driven viscoelastic jets: modeling and experiments. *Korea-Australia Rheology Journal* 20 (3), 153–164.
- [10] Doshi, J., Reneker, D., 1995. Electrospinning process and applications of electrospun fibers. *Journal of electrostatics* 35 (2), 151–160.
- [11] Feng, J., 2002. The stretching of an electrified non-newtonian jet: A model for electrospinning. *Physics of Fluids* 14 (11), 3912–3926.
- [12] Feng, J., 2003. Stretching of a straight electrically charged viscoelastic jet. *Journal of Non-Newtonian Fluid Mechanics* 116 (1), 55–70.
- [13] Greenfeld, I., Fezzaa, K., Rafailovich, M., E, Z., 2012. Fast x-ray phase-contrast imaging of electrospinning polymer jets: measurements of radius, velocity, and concentration. *Macromolecules* 45, 3616–3626.
- [14] Hohman, M., Shin, M., Rutledge, G., Brenner, M., 2001. Electrospinning and electrically forced jets. I. stability theory. *Physics of Fluids* 13 (8), 2201–2220.
- [15] Hohman, M., Shin, M., Rutledge, G., Brenner, M., 2001. Electrospinning and electrically forced jets. II. applications. *Physics of Fluids* 13 (8), 2221–2236.
- [16] Huang, X., Garcia, M., 1998. A Herschel–Bulkley model for mud flow down a slope. *Journal of fluid mechanics* 374, 305–333.
- [17] Mannarino, M., Rutledge, G., 2012. Mechanical and tribological properties of electrospun pa 6(3)t fiber mats. *Polymer* 53, 3017–3025.

- [18] Pisignano, D., 2013. Polymer nanofibers. Cambridge: Royal Society of Chemistry.
- [19] Pontrelli, G., 1997. Mathematical modelling for viscoelastic fluids. *Nonlinear Analysis, Theory, Methods & Applications* 30 (1), 349–357.
- [20] Pontrelli, G., Ubertini, S., Succi, S., 2009. The unstructured lattice boltzmann method for non-newtonian flows. *J. Stat. Mech.: Theory & Exp.* P06005.
- [21] Reneker, D., Yarin, A., Fong, H., Koombhongse, S., 2000. Bending instability of electrically charged liquid jets of polymer solutions in electrospinning. *Journal of Applied physics* 87 (9), 4531–4547.
- [22] Spivak, A., Dzenis, Y., Reneker, D., 2000. A model of steady state jet in the electrospinning process. *Mechanics research communications* 27 (1), 37–42.
- [23] Theron, S., Yarin, A., Zussman, E., Kroll, E., 2005. Multiple jets in electrospinning: experiment and modeling. *Polymer* 46 (9), 2889–2899.
- [24] Yarin, A., Koombhongse, S., Reneker, D., 2001. Bending instability in electrospinning of nanofibers. *Journal of Applied Physics* 89 (5), 3018–3026.

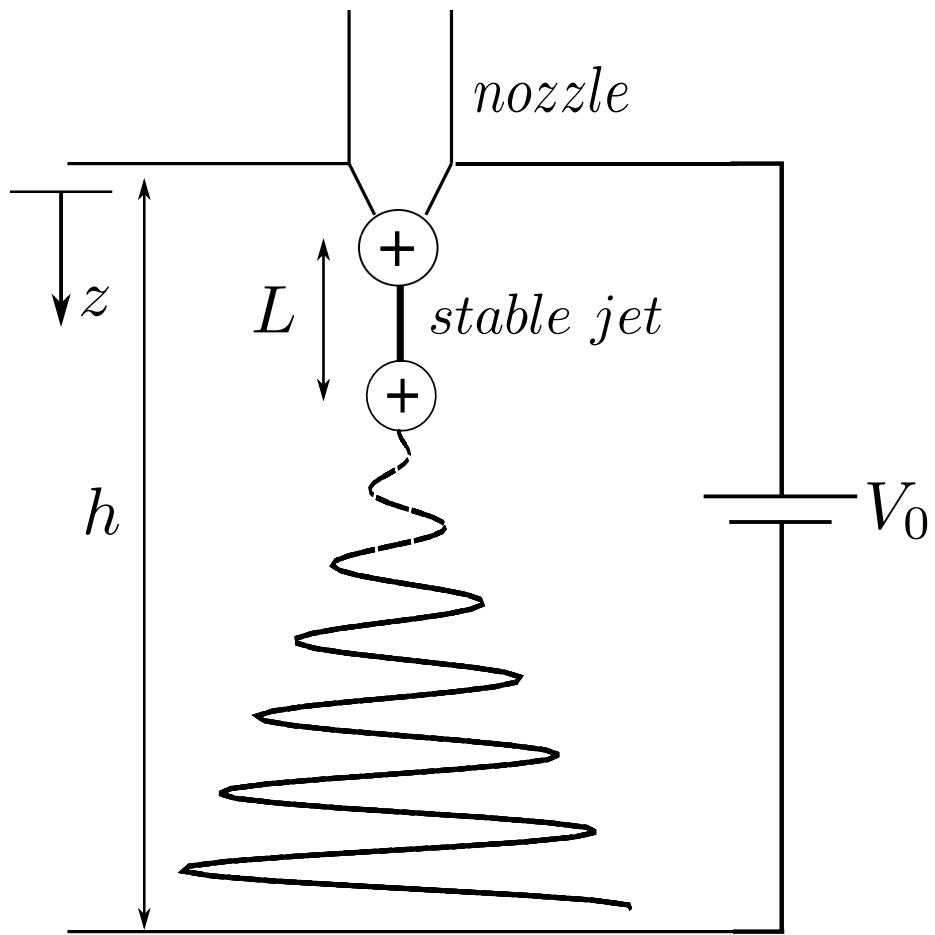


Figure 1: The experimental set up and reference system of the stable jet region, with the origin at the nozzle orifice and z coordinate axis pointing down (figure not to scale).

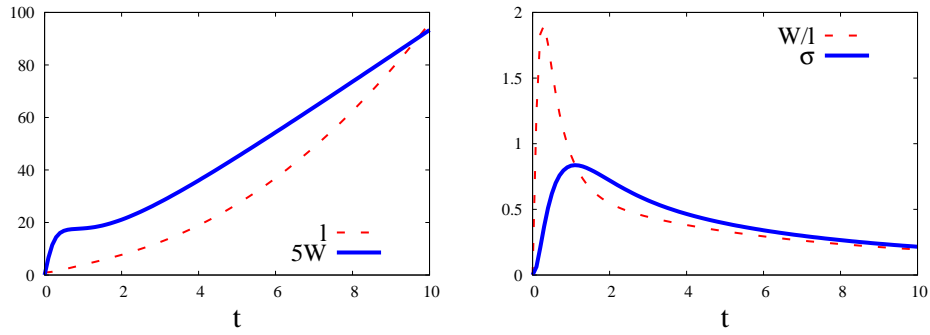


Figure 2: Time evolution of the elongation $l(t)$ and the velocity $5 \cdot W(t)$ (left), the stress $\sigma(t)$ and the strain rate W/l (right) in the Maxwellian case $n = 1, \sigma_Y = 0$ (see text).

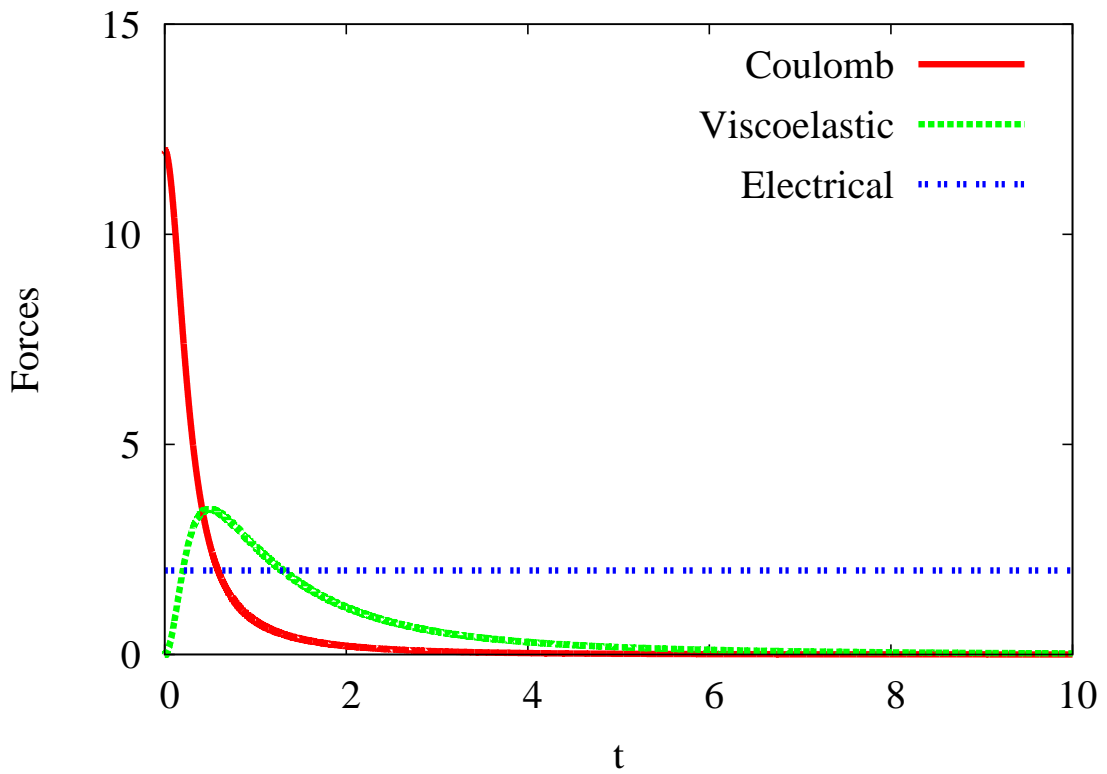


Figure 3: The contribution of the repulsive Coulomb, the (opposite) viscoelastic and the electrical forces as a function of time on the system described by eqn. (2.7) for $n = 1, \sigma_Y = 0$ (see text).

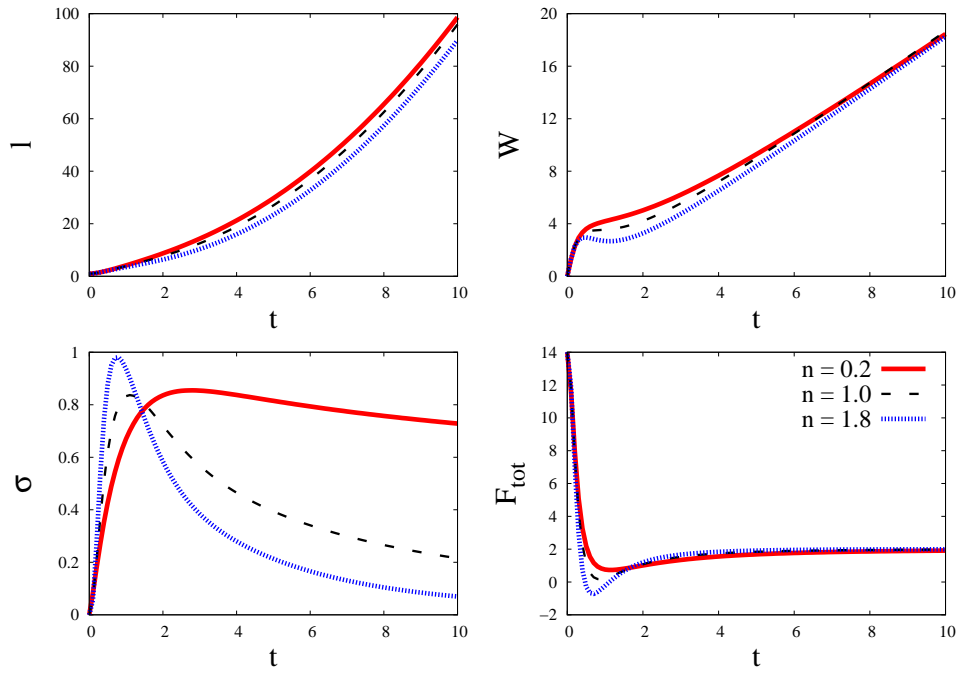


Figure 4: The elongation, the velocity, the stress and the total force of the dimer as a function of time for three values of n ($\sigma_Y = 0$). For $n > 1$, the dimer undergoes a shorter elongation and velocity because in the transient $W/l > 1$ and consequently the case $n > 1$ corresponds to a larger stress than $n = 1$.

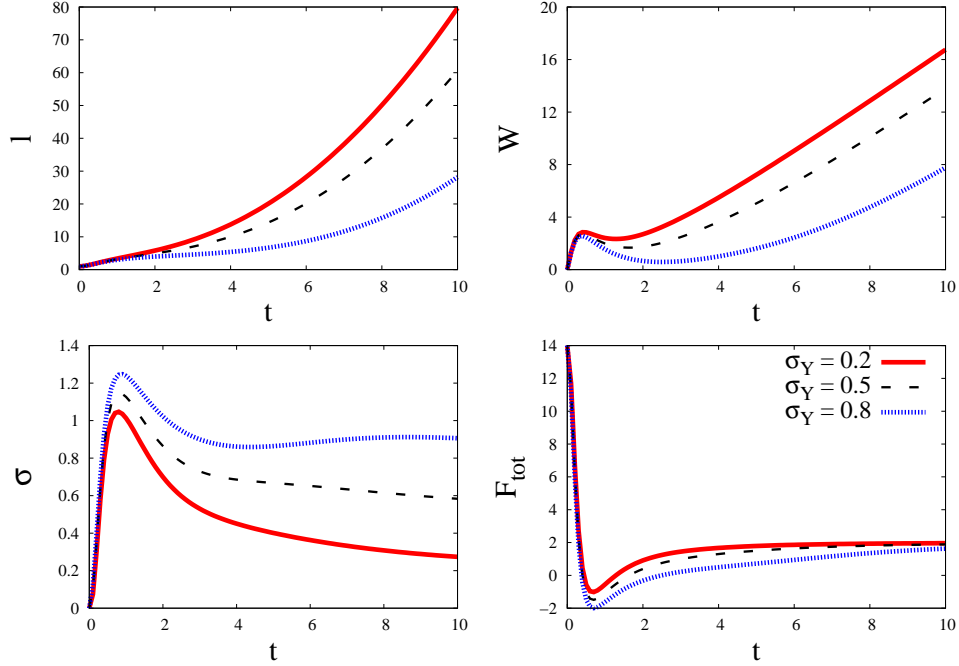


Figure 5: The effect of the yield stress σ_Y on the elongation, the velocity, the stress and total forces ($n = 1.8$); Increasing the value of σ_Y turns out to produce a significant reduction of the fluid elongation.

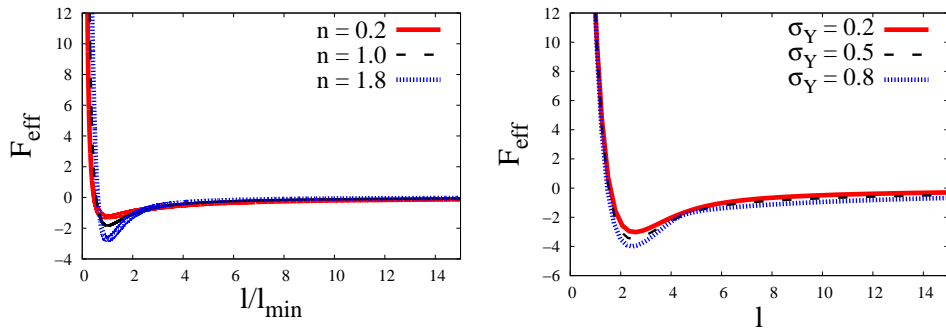


Figure 6: Effective forces as a function of the elongation l for different values of n (left) at $\sigma_Y = 0$, and for different σ_Y at $n = 1$ (right). Note that in the left panel the elongation has been rescaled in units of l_{min} .